第 35 卷第 7 期
2019 年 7 月

无 机 化 学 学 报
CHINESE JOURNAL OF INORGANIC CHEMISTRY

Vol.35 No.7
1283-1294

两个基于双 salamo 型配体的镍(Ⅱ)和锌(Ⅱ)配合物的合成、结构、Hirshfeld 分析和荧光性质

刘玲芝 于 盟 李肖妍 康全鹏 董文魁*
(兰州交通大学化学与生物工程学院,兰州 730070)

摘要: 合成了 2 个新的基于双(salamo)型配体 H_4L 的镍(Ⅱ)和锌(Ⅱ)配合物$[Ni_3(L)(\mu\text{-}OAc)_2(CH_3OH)_3]\cdot CH_3OH\cdot 0.25CHCl_3$ (**1**)和 $[Zn_3(L)(\mu\text{-}OAc)_2(CH_3OH)(H_2O)]\cdot 2CH_3OH$ (**2**),并通过元素分析、红外光谱、紫外-可见吸收光谱、X 射线单晶衍射、热稳定性(TGA)和 Hirshfeld 表面分析对其进行了结构表征。X 射线晶体学分析表明:配合物 **1** 为非对称三核构型,其 3 个镍(Ⅱ)原子均为六配位,形成了一个稍微扭曲的八面体构型,而配合物 **2** 是一个对称的三核结构,中心的锌(Ⅱ)原子是六配位的,具有一种扭曲的八面体构型,与众不同的是另外 2 个锌(Ⅱ)原子是五配位的,表现为扭曲的三角双锥构型。此外,配合物 **1** 和 **2** 通过氢键和 C–H$\cdots\pi$ 相互作用形成了三维超分子结构。最特别的是,配合物 **1** 和 **2** 的荧光性质截然不同。

关键词: 双 salamo 型配体; 配合物; 合成; Hirshfeld 分析; 荧光性质
中图分类号: O614.81$^+$3; O614.24$^+$1　　**文献标识码**: A　　**文章编号**: 1001-4861(2019)07-1283-12
DOI:10.11862/CJIC.2019.158

Syntheses, Structures, Hirshfeld Analyses and Fluorescent Properties of Two Ni(Ⅱ) and Zn(Ⅱ) Complexes Constructed From a Bis(salamo)-like Ligand

LIU Ling-Zhi　YU Meng　LI Xiao-Yan　KANG Quan-Peng　DONG Wen-Kui*
(*School of Chemical and Biological Engineering, Lanzhou Jiaotong University, Lanzhou* 730070, *China*)

Abstract: Two new homo-trinuclear Ni(Ⅱ) and Zn(Ⅱ) complexes, $[Ni_3(L)(\mu\text{-}OAc)_2(CH_3OH)_3]\cdot CH_3OH\cdot 0.25CHCl_3$ (**1**) and $[Zn_3(L)(\mu\text{-}OAc)_2(CH_3OH)(H_2O)]\cdot 2CH_3OH$ (**2**) with a newly synthesized C-type bis(salamo)-like ligand H_4L have been prepared and structurally characterized. The structures of complexes **1** and **2** were fully characterized by elemental analyses, FT-IR, UV-visible spectroscopy, single crystal X-ray crystallography, thermal analyses (TGA) and Hirshfeld surfaces analyses, and their luminescence properties were also discussed. The X-ray crystallography analyses demonstrated that complex **1** is an asymmetric trinuclear structure, and all Ni(Ⅱ) ions are hexa-coordinated, forming distorted octahedral geometries. Meanwhile, complex **2** is a symmetric trinuclear structure, the central Zn2 ion is hexa-coordinated and possesses a distorted octahedral coordination geometry. However, the terminal Zn1 and Zn1#1 ions are both penta-coordinated environments and adopt distorted trigonal bipyramidal geometries. In addition, 3D supramolecular architectures of complexes **1** and **2** were formed by hydrogen bonding and C–H$\cdots\pi$ interactions. Most importantly, the fluorescent property of complex **1** is totally different from that of complex **2**. CCDC: 1891627, **1**; 1891628, **2**.

Keywords: bis(salamo)-like ligand; complex; synthesis; Hirshfeld analysis; fluorescence property

收稿日期:2019-01-20。收修改稿日期:2019-04-29。
国家自然科学基金(No.21761018)资助项目。
*通信联系人。E-mail:dongwk@126.com;会员登记号:02M87091161。

0 Introduction

Salen-type ligands and their transition metal, alkaline earth, and rare earth metal complexes[1-5] have been extensively investigated in modern coordination chemistry for several decades[6-10]. Moreover, these complexes have been studied in obtaining biological systems[11-13], ion recognitions[14], supramolecular buildings[15-22], luminescence properties[23-28], catalyses[29], nonlinear optical materials[30], magnetic materials[31]. Recently, a novel salen-type analogue, salamo, has been developed[32-40]. The salamo-like ligands have their attractive properties in supramolecular architectures[41-43], catalyses[44,45], electrochemical conducts[46], luminescent and magnetic materials[47-52], and biological fields[53].

Based on these above views, we have devised and prepared two new homo-trinuclear Ni(Ⅱ) and Zn(Ⅱ) complexes ($[Ni_3(L)(\mu\text{-}OAc)_2(CH_3OH)_3]\cdot CH_3OH\cdot 0.25CHCl_3$ (**1**) and $[Zn_3(L)(\mu\text{-}OAc)_2(CH_3OH)(H_2O)]\cdot 2CH_3OH$ (**2**)) with a flexible and symmetric bis(salamo)-like ligand H_4L. Meanwhile, the fluorescent properties and Hirshfeld surfaces analyses of complexes **1** and **2** were also studied in detail.

1 Experimental

1.1 Materials and physical measurements

All solvents and chemicals were analytical grade and obtained from Tianjin Chemical Reagent Factory. Melting points were measured by a microscopic melting point apparatus made by the Beijing Taike Instrument Limited Company and the thermometer was uncorrected. Elemental (C, H, and N) analyses were performed on a GmbH Variuo EL V3.00 automatic elemental analyzer (Elementar, Berlin, Germany). Elemental analyses for Zn and Ni were obtained using an IRIS ER/S-WP-ICP atomic emission spectrometer (Elementar, Berlin, Germany). ^{1}H NMR spectra were determined using a German Bruker AVANCE DRX-400 spectrometer. IR spectra were recorded on a VERTEX70 FT-IR spectrophotometer, with samples prepared as KBr (500~4 000 cm^{-1}) and CsI (100~500 cm^{-1}) pellets. UV-Vis absorption and fluorescence spectra were recorded on a Shimadzu UV-2550 (Shimadzu, Japan) and Hitachi F-7000 (Hitachi, Tokyo, Japan) spectrometers, respectively. Thermal analyses (TGA) were carried out at a heating rate of 5 ℃·min^{-1} on a ZRY-1P thermoanalyzer. X-ray single crystal structure determinations of complexes **1** and **2** were carried out on a Bruker APEX-Ⅱ CCD (Bruker AVANCE, Billerica, MA, USA) and SuperNova(Dual, Cu at zero) Eos diffractometers, respectively. The Hirshfeld surfaces analyses of complexes **1** and **2** were calculated using Crystal Explorer program.

1.2 Synthesis of the ligand H_4L

2,3-Dihydroxynaphthalene-1,4-dicarbaldehyde and 1,2-bis(aminooxy)ethane were synthesized according an analogous reported procedure[41,44,47]. Major synthetic route to the ligand H_4L are presented in Scheme 1.

2-Hydroxy-5-nitrobenzaldehyde (341.6 mg, 2.01 mmol) dissolved in ethanol solution (50 mL) was added slowly to a colorless ethanol solution (20 mL) of 1,2-bis(aminooxy)ethane (280.2 mg, 3.00 mmol) for more than 3 h. Subsequently, the above solution was heated at *ca.* 55 ℃ for about 4 h. The solution was concentrated by vacuum distillation. Then, the reaction mixture was separated by column chromatography with ethyl acetate/chloroform (1∶15, *V*/*V*) and expected intermediate product 2-(*O*-(1-ethyloxyamide))oxime-5-nitrophenol was gained.

A nucleophilic addition reaction between 2,3-

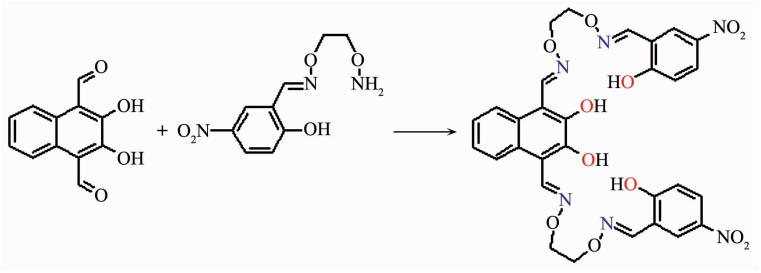

Scheme 1 Synthetic route to H_4L

dihydroxynaphthalene-1,4-dicarbaldehyde and 2-(*O*-(1-ethyloxyamide))oxime-5-nitrophenol was performed according to the previously literature[39]. The orange solid of 2,3-dihydroxynaphthalene-1,4-dicarbaldehyde (216.19 mg, 1 mmol) and the yellowish solid of 2-(*O*-(1-ethyloxyamide))oxime-5-nitrophenol (482.14 mg, 2 mmol) were ground respectively, and then dissolved in absolute ethanol (20 mL). After the mixture was heated under reflux at *ca.* 60 ℃ for 6 h, yellow precipitate was formed. A part of the solvent was removed under reduced pressure to obtain the crude products, which were filtered and washed several times with *n*-hexane to obtain the desired yellow crystalline product of H_4L. Yield: 82.0%. m.p. 166~168 ℃. Anal. Calcd. for $C_{30}H_{26}N_6O_{12}$ (%): C, 54.38; H, 3.96; N, 12.68. Found (%): C, 54.50; H, 3.90; N, 12.47.

1.3 Synthesis of complex 1

A solution of nickel(Ⅱ) acetate tetrahydrate (7.47 mg, 0.03 mmol) in methanol (2 mL) was added to a stirring solution of the ligand H_4L (6.62 mg, 0.01 mmol) in chloroform (3 mL) at room temperature. The color of the mixed solution immediately turned yellow-green. The mixture was filtered and the filtrate was allowed to stay in room temperature for slow evaporation. After about several days, several transparent block-shaped crystals suitable for X-ray measurements were obtained. Yield: 78.5%. Anal. Calcd. for $[Ni_3(L)(\mu\text{-}OAc)_2(CH_3OH)_3]\cdot CH_3OH\cdot 0.25CHCl_3$ ($C_{38.25}H_{44.25}Cl_{0.75}Ni_3N_6O_{20}$) (%): C 41.36; H 4.02; N 7.57; Ni 15.85. Found(%): C 41.49; H 4.11; N 7.47; Ni 15.76.

1.4 Synthesis of complex 2

To a stirred solution of H_4L (6.62 mg, 0.01 mmol) in absolute $CHCl_3$ (2 mL) were added a solution of zinc(Ⅱ) acetate tetrahydrate (6.60 mg, 0.03 mmol) in absolute methanol (3 mL). The mixture was filtered after proper stirring for 10 min and the clear pale yellow solution was then cooled to room temperature. After allowed standing at room temperature for two weeks, yellow crystals suitable for X-ray diffraction analyses were collected. Yield: 62.9%. Anal. Calcd. for $[Zn_3(L)(\mu\text{-}OAc)_2(CH_3OH)(H_2O)]\cdot 2CH_3OH$ ($C_{37}H_{42}Zn_3N_6O_{20}$)(%): C 40.89; H 3.90; N 7.73; Zn 18.05. Found (%): C 41.03; H 3.84; N 7.67; Zn 17.96.

1.5 Crystal structure determinations of complexes 1 and 2

Suitable crystals of complexes **1** and **2** with approximate dimensions of 0.16 mm×0.17 mm×0.22 mm and 0.14 mm×0.15 mm×0.17 mm were performed on a Bruker APEX-Ⅱ CCD diffractometer with a graphite monochromated Mo $K\alpha$ radiation source (λ= 0.071 073 nm) at 153(2) K and SuperNova (Dual, Cu at zero) Eos diffractometer using a graphite monochromated Cu $K\alpha$ radiation source (λ=0.154 184 nm) at 173.00(10) K, respectively. Diffraction data were collected by "multi-scan" mode. Semi-empirical absorption corrections were applied using SADABS (complex **1**) and CrysAlisPro (complex **2**) programs. The structures were solved by direct methods using refined with SHELXL-2015[54]. All hydrogen atoms were added theoretically and difference-Fourier map revealed the positions of the remaining atoms. All non-hydrogen atoms were refined anisotropically using a full-matrix least-squares procedure on F^2 with SHELXL-2014[54]. The crystal data and experimental parameters relevant to the structure determinations are listed in Table 1.

CCDC: 1891627, **1**; 1891628, **2**.

Table 1　Crystal and refinement parameter data for complexes 1 and 2

Complex	1	2
Formula	$C_{38.25}H_{44.25}Cl_{0.75}Ni_3N_6O_{20}$	$C_{37}H_{42}Zn_3N_6O_{20}$
Formula weight	1 110.76	1 086.87
Temperature / K	153(2)	173(10)
Crystal system	Triclinic	Tetragonal
Space group	$P\bar{1}$	$I4_1$
a / nm	1.250 99(7)	1.931 492(17)
b / nm	1.285 63(7)	1.931 492(17)

Continued Table 1

c / nm	1.498 22(8)	1.268 982(15)
α / (°)	78.145(2)	
β / (°)	86.018(2)	
γ / (°)	73.599(2)	
V / nm^3	2.262 1(2)	4.734 14(10)
Z	2	4
D_c / (g·cm^{-3})	1.631	1.522
μ / mm^{-1}	1.366	2.479
F(000)	1 145	2 216
θ range / (°)	2.180~25.024	6.17~69.495
Index ranges	$-14 \leqslant h \leqslant 13, -15 \leqslant k \leqslant 15, -17 \leqslant l \leqslant 17$	$-23 \leqslant h \leqslant 23, -23 \leqslant k \leqslant 21, -15 \leqslant l \leqslant 15$
Reflection collected	16 569	42 004
Independent reflection	7 930	4 431
R_{int}	0.032 3	0.036 7
Completeness to θ / %	99.4	99.5
Data, restraint, parameter	7 930, 48, 650	4 431, 7, 325
GOF on F^2	1.039	1.112
Final R indices [$I>2\sigma(I)$]	R_1=0.048 9, wR_2=0.132 9	R_1=0.038 1, wR_2=0.110 3
Largest diff. peak and hole / (e·nm^{-3})	1 409 and −512	343 and −369

2 Results and discussion

2.1 Crystal structure of complex 1

Single-crystal X-ray diffraction analysis reveals that complex **1** is an asymmetric homo-trinuclear compound, which crystallizes in a triclinic system, space group $P\bar{1}$ with Z=2. The crystal structure of complex **1** and the coordination environment of Ni(Ⅱ) ions are shown in Fig.1. Selected bond lengths and angles of complex **1** are listed in Table 2.

Detailed structural analysis reveals that complex **1** is self-assembled by the coordination of three Ni(Ⅱ) ions, a fully deprotonated ligand L^{4-} unit, two μ-acetato ions, three coordinated methanol molecules, one lattice methanol and a quarter of chloroform molecules. In the crystal structure of complex **1**, two μ-acetato ions bridge three Ni(Ⅱ) ions in a μ-fashion, which probably contributes to the cooperative formation of complex **1**. The terminal Ni1 ion is hexa-coordinated, which occupies the N_2O_2 cavity from the L^{4-} unit and one μ-acetato oxygen atom (O16) and one oxygen atom (O18) of the methanol molecule, forming a distorted octahedral geometry. The Ni3 ion has above similar coordination environment and

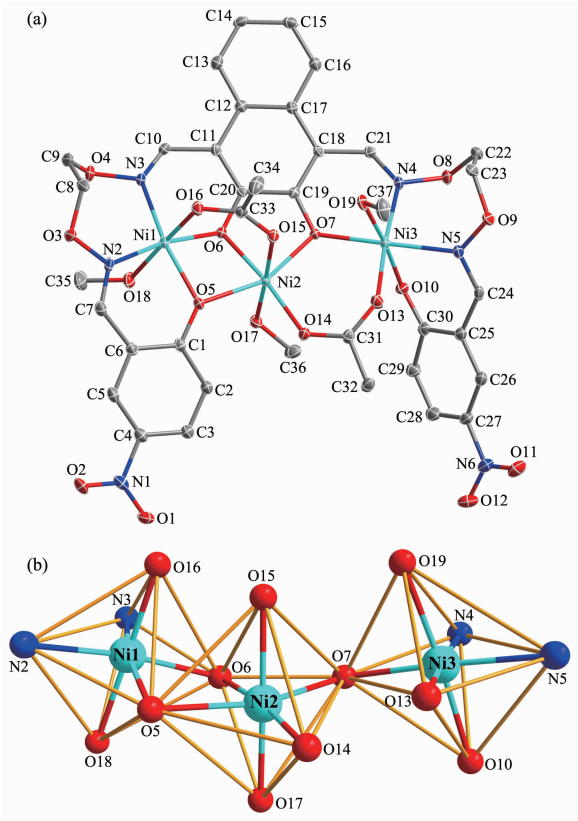

Hydrogen atoms and solvent molecules are omitted for clarity

Fig.1 (a) Molecular structure of complex **1** with 30% probability displacement ellipsoids; (b) Coordination polyhedrons for the Ni(Ⅱ) ions

coordination geometry. Meanwhile, the central Ni2 ion is held by an O_6 cavity provided by three oxygen coordination sites of the L^{4-} unit in assistance of two μ-acetato oxygen atoms (O14 and O15) and one oxygen atom (O17) from the methanol molecule to form a distorted octahedral geometry.

Ni1 and Ni2 ions are bridged by O15 and O16 atoms with a Ni1…Ni2 distance of 0.303 53(6) nm,

Table 2　Selected bond distances (nm) and angles (°) for complexes 1 and 2

1					
N2-Ni1	0.204 2(4)	Ni1-O16	0.204 2(3)	Ni2-O7	0.208 9(3)
N3-Ni1	0.202 5(4)	Ni1-O18	0.212 6(3)	Ni2-O5	0.212 1(3)
N4-Ni3	0.202 0(4)	Ni2-O14	0.197 1(2)	Ni3-O13	0.202 2(3)
N5-Ni3	0.210 4(3)	Ni2-O6	0.198 7(3)	Ni3-O7	0.255(3)
Ni1-O6	0.199 8(3)	Ni2-O15	0.207 2(3)	Ni3-O10	0.205 7(3)
Ni1-O5	0.200 6(2)	Ni2-O17	0.207 0(3)	Ni3-O19	0.214 7(3)
O6-Ni1-O5	81.85(11)	O14-Ni2-O6	172.63(12)	O7-Ni3-O19	83.75(12)
O6-Ni1-N3	84.96(14)	O14-Ni2-O15	96.53(13)	O10-Ni3-O19	174.27(12)
O5-Ni1-N3	166.48(15)	O6-Ni2-O15	89.55(12)	N5-Ni3-O19	100.10(14)
O6-Ni1-O16	91.62(12)	O14-Ni2-O17	86.64(13)	N4-Ni3-O13	174.64(13)
O5-Ni1-O16	90.66(13)	O6-Ni2-O17	87.31(12)	N4-Ni3-O7	85.66(12)
N3-Ni1-O16	92.69(15)	O15-Ni2-O17	176.82(12)	O13-Ni3-O7	99.20(11)
O6-Ni1-N2	169.71(13)	O14-Ni2-O7	105.03(11)	N4-Ni3-O10	93.27(14)
O5-Ni1-N2	88.65(13)	O6-Ni2-O7	79.57(11)	O13-Ni3-O10	88.65(13)
N3-Ni1-N2	104.28(15)	O15-Ni2-O7	85.05(12)	O7-Ni3-O10	94.35(12)
O16-Ni1-N2	92.44(14)	O17-Ni2-O7	93.92(12)	N4-Ni3-N5	91.33(14)
O6-Ni1-O18	89.66(13)	O14-Ni2-O5	96.67(12)	O13-Ni3-N5	83.96(13)
O5-Ni1-O18	87.35(12)	O6-Ni2-O5	79.29(11)	O7-Ni3-N5	175.21(15)
N3-Ni1-O18	89.60(15)	O15-Ni2-O5	88.34(12)	O10-Ni3-N5	82.08(14)
O16-Ni1-O18	177.46(13)	O17-Ni2-O5	91.52(12)	N4-Ni3-O19	91.99(14)
N2-Ni1-O18	85.94(15)	O7-Ni2-O5	157.88(11)	O13-Ni3-O19	86.32(13)
2					
Zn1-O1	0.196 3(4)	Zn1-N3	0.204 7(5)	Zn2-O8#1	0.204 9(4)
Zn1-O6#1	0.208 3(3)	Zn2-O6	0.208 3(3)	Zn2-O9	0.213 3(4)
Zn1-O7	0.197 0(4)	Zn2-O6#1	0.208 3(3)	Zn2-O9#1	0.213 3(4)
Zn1-N2	0.218 2(5)	Zn2-O8	0.204 9(4)		
O1-Zn1-O6	92.17(15)	N3-Zn1-N2	89.03(19)	O8#1-Zn2-O6#1	92.85(14)
O1-Zn1-O7	120.87(19)	O6-Zn2-O6#1	77.81(18)	O8-Zn2-O6	92.85(14)
O1-Zn1-N2	85.4 (2)	O6#1-Zn2-O9#1	87.70 (16)	O8#1-Zn2-O8	97.1(2)
O1-Zn1-N3	117.88(18)	O6-Zn2-O9#1	94.62(17)	O8-Zn2-O9	91.40(18)
O6-Zn1-N2	169.89(17)	O6#1-Zn2-O9	94.62(17)	O8#1-Zn2-O9	86.63(17)
O7-Zn1-O6	94.58(16)	O6-Zn2-O9	87.69(16)	O8-Zn2-O9#1	86.63(17)
O7-Zn1-N2	95.09(19)	O8-Zn2-O6#1	168.64(15)	O8#1-Zn2-O9#1	91.40(18)
O7-Zn1-N3	121.25(19)	O8#1-Zn2-O6	168.64(15)	O9-Zn2-O9#1	177.0(3)
N3-Zn1-O6	83.46(14)				

Symmetry codes: #1: 1−x, 1−y, z for **2**.

and Ni2 and Ni3 ions are bridged by O13 and O14 atoms with a Ni2⋯Ni3 distance of 0.350 02(4) nm. The bond distances of Ni-O are in a range of 0.197 1(2)~0.214 9(2) nm, and the average distance of Ni-O bonds is 0.205 45 nm. A stable chelating Ni(Ⅱ) complex is formed between H_4L and the Ni(Ⅱ) ions, while the methanol molecules bind to the Ni(Ⅱ) ions, which result in the enhancement of the inflexibility and the formation of two perpendicularly crossing planes.

Intermolecular interactions, especially classical and non-classical hydrogen bondings, are playing a crucial role in the formation of crystalline solids and their physiochemical properties. The hydrogen bonding interactions are listed in Table 3 and the packing arrangement of molecules is represented in Fig.3. As illustrated in Fig.2, seven pairs of intramolecular hydrogen bondings are formed. Furthermore, a 3D supramolecular network structure of complex **1** is composed of two parts[55-59]. The first part is linked by five pairs of intermolecular hydrogen bondings. It is worth noting that another part is linked by C–H⋯π (C32–H32C⋯Cg1 (Cg1: C25-C26-C27-C28-C29-C30) interactions[25].

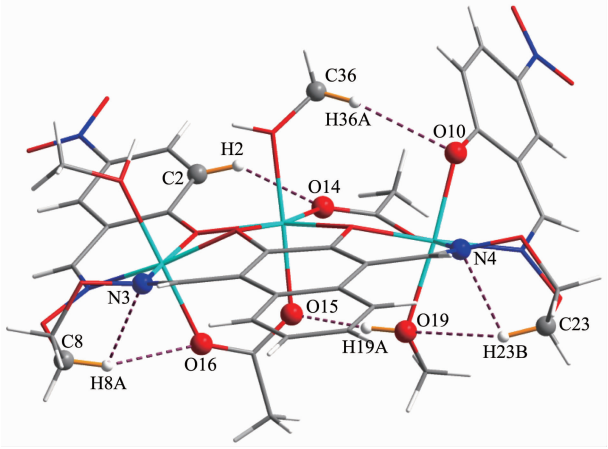

Fig.2 View of intramolecular hydrogen bonding interactions of complex **1**

Table 3 Hydrogen bonding and C–H⋯π interactions of complexes 1 and 2

D–H⋯A	*d*(D-H) / nm	*d*(H⋯A) / nm	*d*(D⋯A) / nm	∠DHA / (°)
		1		
O19–H19A⋯O15	0.091	0.177 0	0.268 4(3)	175
C2–H2⋯O14	0.095	0.231 0	0.310 0(5)	140
C5–H5⋯O11#1	0.095	0.258 0	0.342 2(6)	148
C8–H8A⋯O16	0.099	0.233 0	0.325 9(5)	156
C8–H8A⋯N3	0.099	0.250 0	0.283 9(4)	100
C8–H8B⋯O2#2	0.099	0.238 0	0.335 0(7)	166
C9–H9B⋯O1#3	0.099	0.235 0	0.324 7(6)	150
C22–H22B⋯O2#4	0.099	0.245	0.319 2(6)	131
C23–H23B⋯O19	0.099	0.238	0.329 6(5)	153
C23–H23B⋯N4	0.099	0.247	0.282 1(7)	101
C24–H24⋯O3#5	0.095	0.259	0.337 0(5)	139
C36–H36A⋯O10	0.098	0.259	0.354 3(5)	164
C32–H32C⋯Cg1	—	0.283 0	0.353 7(4)	126
		2		
O9–H9A⋯O4	0.084	0.189	0.264 6(6)	150
C10–H10⋯O5#2	0.093	0.237	0.323 7(9)	156
C14–H14⋯O5#2	0.093	0.243	0.321 0(11)	142
C18–H18B⋯O6#3	0.096	0.180	0.234(3)	128
C18–H18B⋯O11	0.096	0.245	0.314 4(2)	112
C9–H9B⋯Cg2#4	—	0.278 0	0.314(3)	103

Symmetry codes: #1: *x*, *y*, −1+*z*; #2: 1−*x*, 1−*y*, −*z*; #3: *x*, −1+*y*, *z*; #4: *x*, −1+*y*, 1+*z*; #5: *x*, *y*, 1+*z* for **1**; #2: 1/2−*x*, 1/2−*y*, −1/2+*z*; #3: 1−*x*, 1−*y*, *z*; #4: 1/2+*x*, 1−*y*, 1/4+*z* for **2**; Cg1 is the centroids of benzene ring C25-C26-C27-C28-C29-C30 of **1**; Cg2 is the centroids of benzene ring C13-C14-C15-C15a-C14a-C13a of **2**.

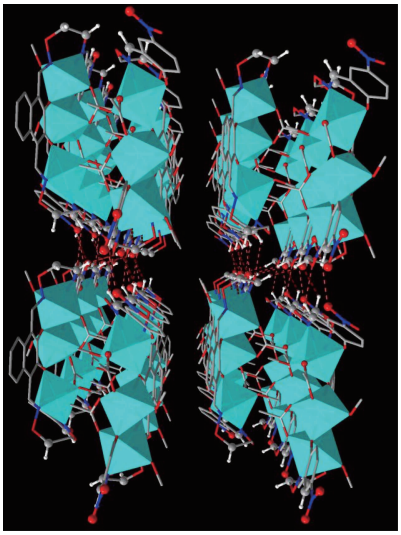

Fig.3　Three dimensional supramolecular architecture of complex **1** by hydrogen bonding and C–H···π interactions

2.2　Crystal structure of complex 2

The crystal structure and atom numberings of complex **2** was determined by X-ray crystallography and is shown in Fig.4. Selected bond lengths and angles of complex **2** are listed in Table 2.

Single crystal X-ray diffraction analysis indicates that complex **2** crystallizes in a tetragonal crystal system, space group $I4_1$, and consists of three Zn(Ⅱ) ions, one L^{4-} unit, two μ-acetato ions, one coordinated methanol and water molecules and two lattice methanol molecules.

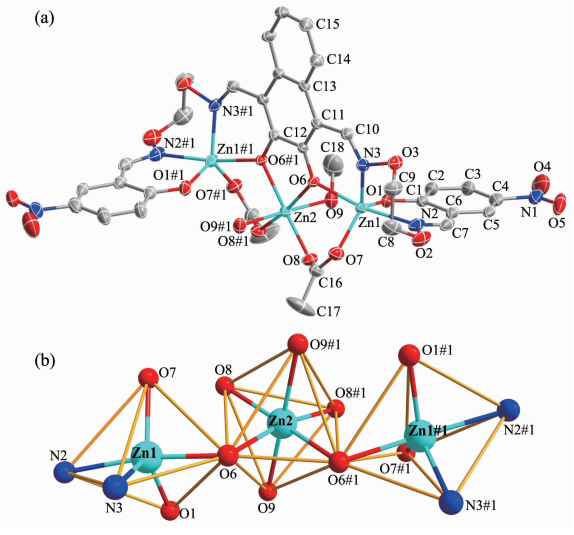

Hydrogen atoms and solvent molecules are omitted for clarity; Symmetry codes: #1: $-x$, $1-y$, z

Fig.4　(a) Molecular structure of complex **2** with 30% probability displacement ellipsoids; (b) Coordination polyhedrons for the Zn(Ⅱ) ions

In the crystal structure of complex **2**, we can see that the coordination ratio of the ligand L^{4-} unit to Zn(Ⅱ) ion is 1:3[47]. Meanwhile, two terminal Zn(Ⅱ) ions (Zn1 and Zn1#1) are located in the N_2O_2 cavities and the axial positions are occupied by O7 and O7#1 from two μ-acetato ions. They are both in penta-coordinated environments and adopt distorted trigonal bipyramidal geometries, which was inferred by calculating the value of τ_{Zn1}=0.81[40]. The central O_6 site(O6 and O6#1 from L^{4-}; O8 and O8#1 from μ-acetato ions; O9 and O9#1 from methanol and water molecules, respectively) is occupied by one Zn2 ion, which is hexa-coordinated with a distorted octahedral geometry influenced by Jahn-Teller effect. Two terminal Zn(Ⅱ) ions (Zn1 and Zn1#1) connect central Zn2 ion via a familiar Zn-O-Zn-O-Zn fashion with O6 and O6#1 from L^{4-} unit as a "bridge". The coordination between the ligand L^{4-} unit and three Zn(Ⅱ) ions gives rise to a stable chelating complex.

Supramolecular architecture of complex **2** is connected by extensive hydrogen bonding and C–H···π interactions, which plays a major role in the crystal packing modes. In the crystal structure of complex **2**, two pair of intramolecular (C18–H18B···O6 and O9–H9A···O4) hydrogen bonding interactions, two significant intermolecular and one significant C–H···π (C9–H9B ··· Cg2 (Cg2: C13-C14-C15-C15a-C14a-C13a)) interactions help to form a 3D supramolecular structure (Fig.5)[60-63].

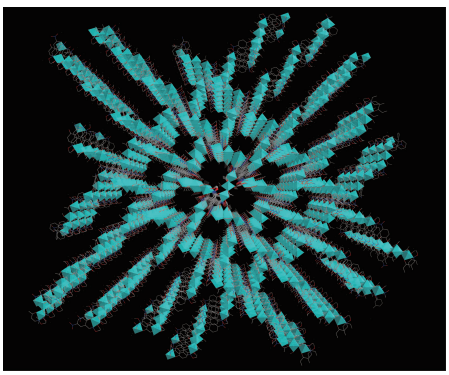

Fig.5　Three dimensional supramolecular architecture of complex **2** by hydrogen bonding and C–H···π interactions

2.3 FT-IR spectra

The FT-IR spectra of H_4L and its corresponding complexes **1** and **2** exhibited various bands in the 4 000~500 cm^{-1} region (Fig.6 and Table 4).

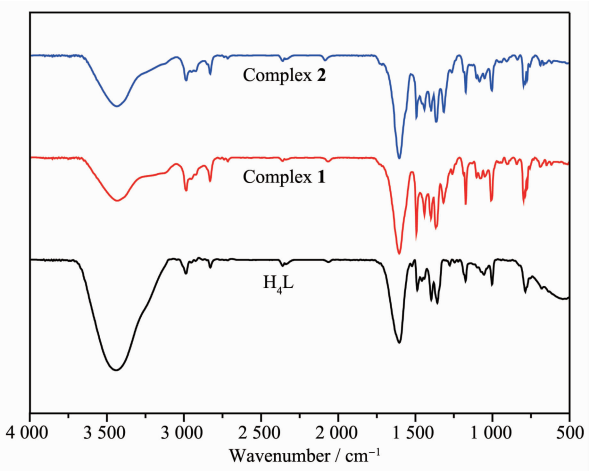

Fig.6 FT-IR spectra of H_4L and its complexes **1** and **2**

The free ligand H_4L exhibited characteristic Ar-O and C=N stretching bands at *ca.* 1 244 and 1 610 cm^{-1}, respectively[48]. Upon complexation, those of complexes **1** and **2** shifted to the lower frequencies, which give therefore a proof of the coordination of oxime nitrogen and phenolic oxygen to the Ni(Ⅱ) and Zn(Ⅱ) ions. It can be seen from the Fig.6 that the phenolic O-H stretching vibration band of free ligand H_4L exhibited the expected absorption band at *ca.* 3 430 cm^{-1}, whereas this band disappeared in complexes **1** and **2**, indicating that the hydroxyl groups of phenolic and naphthalenediol of salamo moieties are completely deprotonated and coordinated with the Ni(Ⅱ) and Zn(Ⅱ) ions. Meanwhile, new O-H vibration bands were observed at 3 445 and 3 435 cm^{-1} in complexes **1** and **2**, which belongs to the coordinated methanol molecules. In addition, the bands at 532, 527 cm^{-1} and 467, 473 cm^{-1} in complexes **1** and **2** are attributed to ν_{M-N}) and ν_{M-O}, respectively[64-67]. These bands are not existed in the spectrum of the free ligand H_4L. The facts mentioned above are in accordance with the results of single crystal X-ray diffractions.

Table 4 Main FT-IR spectra data of H_4L and its complexes 1 and 2

cm^{-1}

Compound	ν_{O-H}	ν_{Ar-O}	$\nu_{C=N}$	$\nu_{C=C}$	ν_{M-O}	ν_{M-N}
H_4L	3 430	1 244	1 610	1 530	—	—
Complex **1**	3 445	1 228	1 596	1 491	467	532
Complex **2**	3 435	1 227	1 604	1 496	473	527

2.4 UV-Vis absorption spectra

We examined the UV-Vis spectra of H_4L in 50 $\mu mol \cdot L^{-1}$ DMF solution at room temperature, and the corresponding Ni(Ⅱ) and Zn(Ⅱ) complexes were analyzed by UV-Vis spectra during addition of aliquots of the transition metal(Ⅱ) ion solutions.

The σ-donor/π-acceptor salamo ligand H_4L showed three characteristic high intensity bands located at λ=341, 358 and 377 nm, which can be assigned to the intra-ligand π-π* transitions[52]. The band at 428 nm is associated with the metal-to-ligand charge transfer (MLCT) transition. These bands are related to the non-resolved *d*-*d* transitions from the four low-lying *d*-orbitals (d_{xz}, d_{yz}, d_{z^2}, $d_{x^2-y^2}$) to the empty (Ni), or filled (Zn) d_{xy} orbital. For the UV-Vis titrations, the measurements were performed in a mixture of DMF aqueous solution due to solubility reasons. Upon the gradual addition of Ni^{2+}/Zn^{2+} to H_4L, the absorbance at 377 nm was steadily enhanced until the amount of Ni^{2+}/Zn^{2+} reached 3 equivalents (Fig.7).

2.5 Fluorescence properties

All the fluorescent determinations were put into effect with an entrance slit and exit slit of 10 and 20 nm, respectively, and excitation wavelength was 410 nm. The fluorescence properties of H_4L and its corresponding complexes **1** and **2** were investigated at room temperature in wavelength range of 400 ~650 nm, as shown in Fig.8.

The spectrum of H_4L exhibited a weak emission peak at *ca.* 490 nm upon excitation at 410 nm, and it should be assigned to the intraligand π-π* transition[40,47]. Complex **1** showed lower photoluminescence

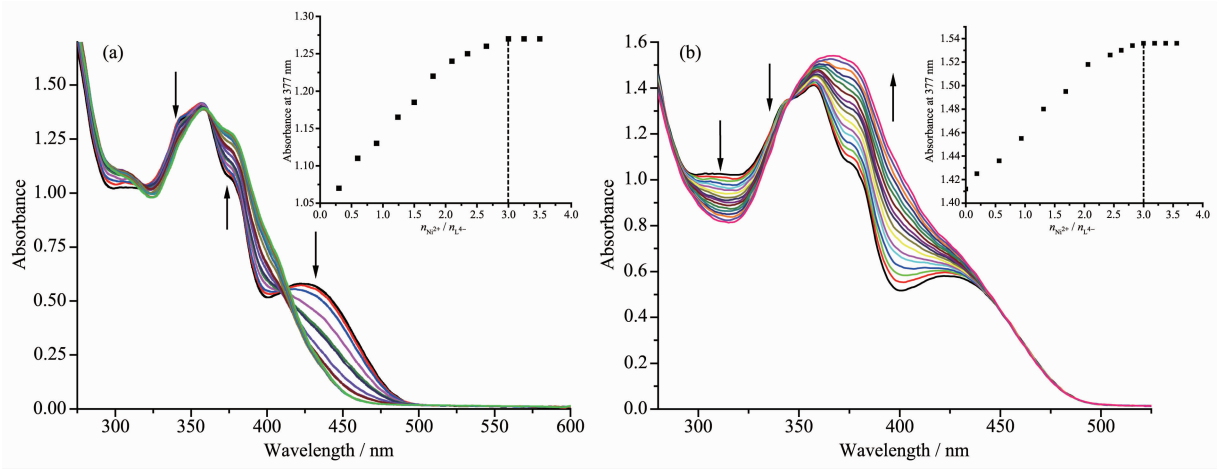

c_1=50 mmol·L^{-1}, $c_{Ni(OAc)_2}$=1mmol·L^{-1}, c_2=50 mmol·L^{-1}, $c_{Zn(OAc)_2}$=1 mmol·L^{-1}

Fig.7　(a) UV-Vis spectral changes of complex **1** of H_4L in DMF by the addition of $Ni(OAc)_2$ in distilled water; (b) UV-Vis spectral changes of complex **2** of H_4L in DMF by the addition of $Zn(OAc)_2$ in distilled water

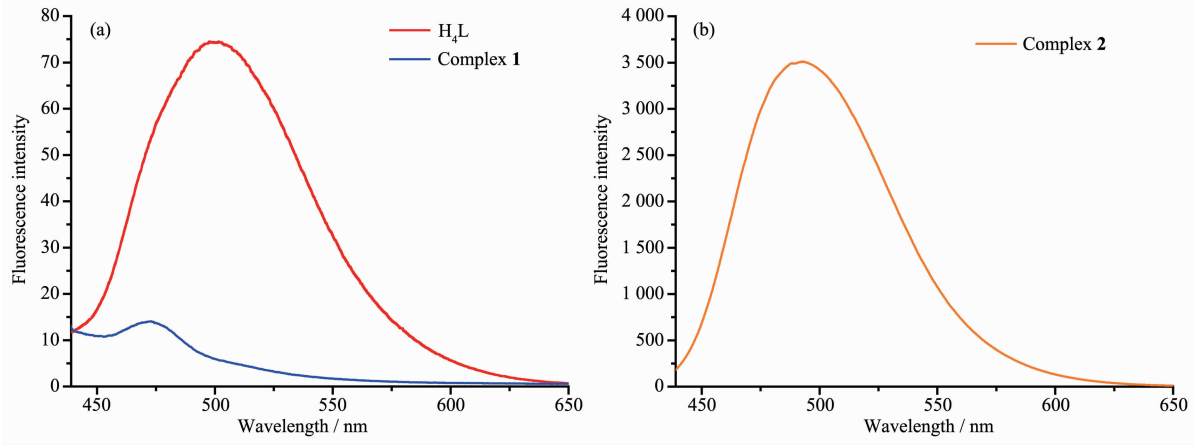

V_{DMF}:$V_{methanol}$=1:9, c=50 μmol·L^{-1}

Fig.8　Emission spectra of H_4L and its complexes **1** and **2** in DMF+methanol

with maximum emission at *ca.* 475 nm. Compared with the ligand H_4L, emission intensity of complex **1** reduces obviously, which indicates that the Ni(Ⅱ) ions have a quality of fluorescent quenching, and makes the conjugated system larger. It is worth noting that complex **2** displayed an intense emission peak at ca. 490 nm when excited at 410 nm. Meanwhile, compared with the ligand H_4L, the emission intensity of complex **2** increased by more than 40 times.

2.6　Hirshfeld surfaces analyses

The Hirshfeld surfaces of H_4L and its complexes **1** and **2** were analyzed using CrystalExplorer program. As shown in Fig.9, the Hirshfeld surfaces analyses[68] of complexes **1** and **2** are illustrated, showing surfaces that have been projected over d_{norm} (standard high resolution), d_e and shape index.

When mapped with the function of d_{norm}, the

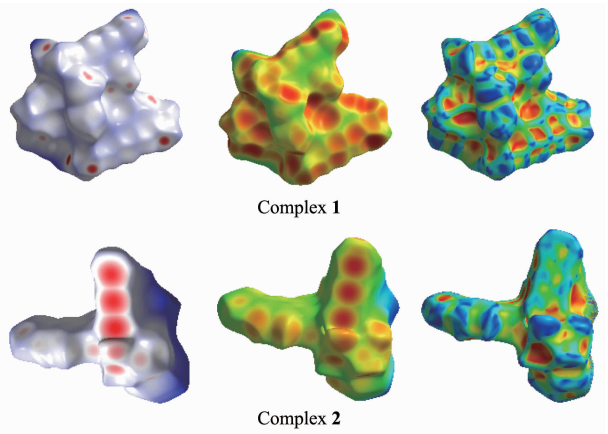

Fig.9　Hirshfeld surfaces of complexes **1** and **2** mapped with d_{norm}, d_e and shape index

surfaces of complexes **1** and **2**, the bright red regions of the depression in the Hirshfeld surface indicate the existence of the O-H interactions, and the light red spots are due to C –H ⋯ O interactions, and other bulging blue regions in the Hirshfeld surface represent C ⋯ H/H ⋯ C, H · · · H and O ⋯ H/H ⋯ O contacts in complexes **1** and **2**.

The 2D plots generated[69] correspond to the O⋯ H, C ⋯ H, C ⋯ C and H ⋯ H interactions from the Hirshfeld surfaces of complexes **1** and **2** are shown in Fig.10. For simplicity and clarity, the outline of the entire fingerprint is shown in gray, and the blue region shows different short-range interactions. For each point on the Hirshfeld isosurface, two distances, d_e (the distance from the point to the nearest nucleus external to the surface) and d_i (the distance to the nearest nucleus internal to the surface), are defined. The proportions of C⋯H/H⋯C, O⋯H/H⋯O and H⋯ H interactions in complexes **1** and **2** cover 16.3% and 12.2%, 27.6% and 32.6%, 37.8% and 38.9% of the Hirshfeld surfaces, respectively. It is because of the existence of these short-range interactions that the complexes can be more stable.

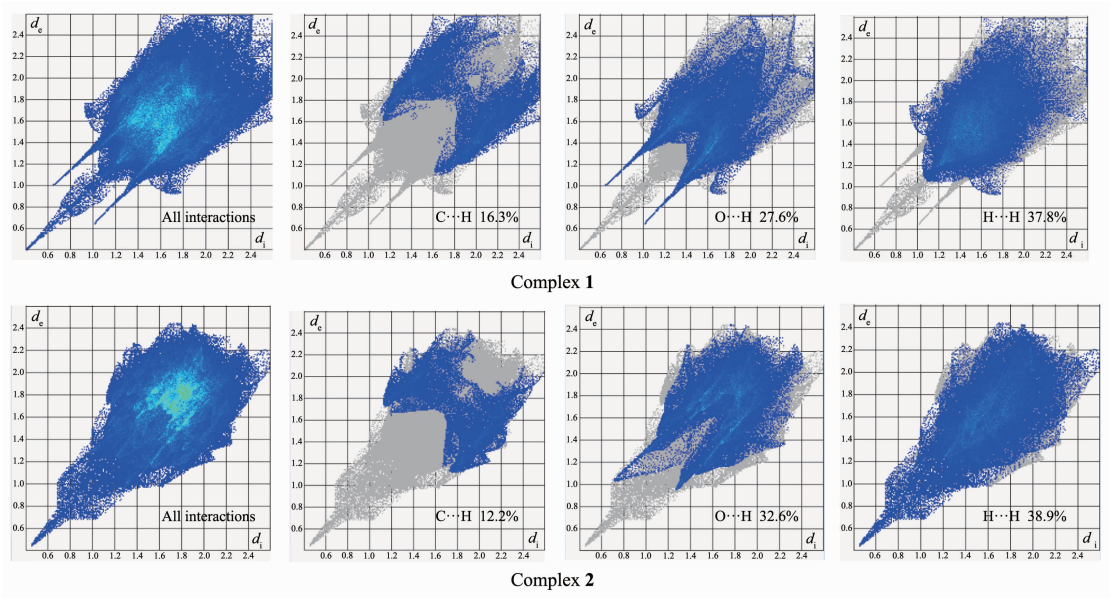

Fig.10 Two dimensional fingerprint plots of complexes **1** and **2** with the major decomposition plots

2.7 Thermal analyses

Thermal stabilities were investigated for complexes **1** and **2**. The TG curve of complex **1** was divided into three stages. The first stage occurred in the 47~91 ℃ range with the weight loss of 5.8%, which is similar to the value (5.6%) estimated for the loss of lattice chloroform and methanol molecules of complex **1**. This result is consistent with the previous element analysis results. The second stage was from 146 to 229 ℃ with a weight loss of 24.3%, which corresponds to the loss of the three coordinated methanol molecules and two μ-acetate ions (Calcd. 24.6%). Finally, the third weight loss starts at around 300 ℃, leading to further decomposition of complex **1**. At about 680 ℃, the TG curve showed an approximately 50.2% total weight loss, indicating the complete removal of the L^{4-} unit. The main residual product was NiO, with a value of 19.7% (Calcd. 20.1%). Similar to complex **1**, the first stage of TG curve for complex **2** occurred in the 56~ 135 ℃ range with the weight loss of 5.6%, which is similar to the value(5.9%) estimated for the loss of the lattice methanol molecules of complex **2**. And the main residual products of complex **2** was ZnO, with a value of 22.7% (Calcd. 22.5%).

3 Conclusions

Two new homo-trinuclear Ni(Ⅱ) and Zn(Ⅱ) complexes, $[Ni_3(L)(\mu\text{-}OAc)_2(CH_3OH)_3]\cdot CH_3OH\cdot 0.25CHCl_3$ (**1**) and $[Zn_3(L)(\mu\text{-}OAc)_2(CH_3OH)(H_2O)]\cdot 2CH_3OH$ (**2**) with a flexible bis (salamo)-like ligand H_4L have been

prepared and structurally characterized. Complexes **1** and **2** were fully characterized by elemental analyses, FT-IR, UV-visible spectra, single crystal X-ray crystallography, Hirshfeld surfaces analyses, and their luminescence properties were also discussed. Infinite 3D supramolecular architectures of complexes **1** and **2** were formed by hydrogen bonding and C –H ··· π interactions. Most importantly, the fluorescent property of complex **1** is totally different from that of complex **2**. Compared with the ligand H_4L, the emission intensity of complex **2** increased by more than 40 times while complex **1** have a quality of fluorescent quenching.

Acknowledgements: This work was supported by the National Natural Science Foundation of China (Grant No. 21761018) and the Program for Excellent Team of Scientific Research in Lanzhou Jiaotong University (Grant No.201706), which are gratefully acknowledged.

References:

[1] Akine S, Varadi Z, Nabeshima T. *Eur. J. Inorg. Chem.*, **2013**, **35**:5987-5998

[2] Sun Y X, Wang X Y, Dong Z L, et al. *Synth. React. Inorg. Met.-Org. Nano-Met. Chem.*, **2013**,**43**:599-603

[3] Wu H L, Bai Y H, Zhang Y H, et al. *Z. Anorg. Allg. Chem.*, **2014**,**640**:2062-2071

[4] Akine S, Miyashita M, Piaob S, et al. *Inorg. Chem. Front.*, **2014**,**1**:53-57

[5] Wu H L, Wang H, Wang X L, et al. *New J. Chem.*, **2014**,**38**: 1052-1061

[6] Song X Q, Peng Y J, Chen G Q, et al. *Inorg. Chim. Acta*, **2015**,**427**:13-21

[7] Song X Q, Liu P P, Liu Y A, et al. *Dalton Trans.*, **2016**,**45**: 8154-8163

[8] Zhou J J, Song X Q, Liu Y A, et al. *RSC Adv.*, **2017**,**7**:25549-25559

[9] Liu P P, Sheng L, Song X Q, et al. *Inorg. Chim. Acta*, **2015**, **434**:252-257

[10]Canaj A B, Siczek M, Otrba M, et al. *Dalton Trans.*, **2016**, **45**:18591-18602

[11]Wang F, Xu Y L, Aderinto S O, et al. *J. Photochem. Photobiol. A*, **2017**,**332**:273-282

[12]Wu H L, Bai Y C, Zhang Y H, et al. *J. Coord. Chem.*, **2014**, **67**:3054-3066

[13]Wu H L, Pan G L, Bai Y C, et al. *Res. Chem. Intermed.*, **2015**,**41**:3375-3388

[14]Yu B, Li C Y, Sun Y X, et al. *Spectrochim. Acta Part A*, **2017**,**184**:249-254

[15]Chai L Q, Zhang K Y, Tang L J, et al. *Polyhedron*, **2017**, **130**:100-107

[16]Chai L Q, Tang L J, Chen L C, et al. *Polyhedron*, **2017**,**122**: 228-240

[17]Zhou L, Hu Q, Chai L Q, et al. *Polyhedron*, **2019**,**158**:102-116

[18]Chai L Q, Hu Q, Zhang K Y, et al. *J. Lumin.*, **2018**,**203**: 234-246

[19]Chai L Q, Huang J J, Zhang H S, et al. *Spectrochim. Acta Part A*, **2014**,**131**:526-531

[20]Chai L Q, Zhang J Y, Chen L C, et al. *Res. Chem. Intermed.*, **2016**,**42**:3473-3488

[21]Chai L Q, Mao K H, Zhang J Y, et al. *Inorg. Chim. Acta*, **2017**,**457**:34-40

[22]Chai L Q, Zhang H S, Huang J J, et al. *Spectrochim. Acta Part A*, **2015**,**137**:661-669

[23]SUN Yin-Xia(孙银霞), LI Chun-Yu(李春宇), YANG Cheng-Juan(杨成娟), et al. *Chinese J. Inorg. Chem.*(无机化学学报), **2016**,**32**:327-335

[24]SUN Yin-Xia(孙银霞), ZHAO Ya-Yuan(赵亚元), LI Chun-Yu(李春宇), et al. *Chinese J. Inorg. Chem.*(无机化学学报), **2016**,**32**:913-920

[25]Sun Y X, Gao X H. *Synth. React. Inorg., Met.-Org. Nano-Met. Chem.*, **2011**,**41**:973-978

[26]Jia H R, Li J, Sun Y X, et al. *Crystals*, **2017**,**7**:247

[27]Jia H R, Chang J, Zhang H J, et al. *Crystals*, **2018**,**8**:272

[28]Li J, Zhang H J, Chang J, et al. *Crystals*, **2018**,**8**:176

[29]Chin T K, Endud S, Jamil S, et al. *Catal. Lett.*, **2013**,**143**: 282-288

[30]Bella S D, Fragala I. *Synth. Met.*, **2000**,**115**:191-196

[31]Song X Q, Liu P P, Xiao Z R, et al. *Inorg. Chim. Acta*, **2015**,**438**:232-244

[32]Wang P, Zhao L. *Synth. React. Inorg. Met.-Org. Nano-Met. Chem.*, **2016**,**46**:1095-1101

[33]Tao C H, Ma J C, Zhu L C, et al. *Polyhedron*, **2017**,**128**:38-45

[34]Zhang Y, Liu L Z, Pan Y Q, et al. *Crystals*, **2018**,**8**:259

[35]Dong X Y, Zhao Q, Kang Q P, et al. *Crystals*, **2018**,**8**:230

[36]Dong X Y, Akogun S F, Zhou W M, et al. *J. Chin. Chem. Soc.*, **2017**,**64**:412-419

[37]Zhang L W, Li X Y, Kang Q P, et al. *Crystals*, **2018**,**8**:173

[38]Li X Y, Kang Q P, Liu L Z, et al. *Crystals*, **2018**,**8**:43

[39]YANG Yu-Hua(杨玉华), HAO Jing(郝静), DONG Yin-Juan(董银娟), et al. *Chinese J. Inorg. Chem.*(无机化学学报), **2017**,**33**:1280-1292

[40]Hao J, Liu L Z, Dong W K, et al. *J. Coord. Chem.*, **2017**,**70**: 1936-1952

[41]Dong W K, Ma J C, Zhu L C, et al. *New J. Chem.*, **2016**,**40**: 6998-7010

[42]PENG Yun-Dong(彭云冬), WANG Fei(王飞), GAO Lei(高垒), et al. *Chinese J. Inorg. Chem.*(无机化学学报), **2018**, **65**:893-899

[43]Dong W K, Ma J C, Dong Y J, et al. *Polyhedron*, **2016**,**115**: 228-235

[44]Chen L, Dong W K, Zhang H, et al. *Cryst. Growth Des.*, **2017**,**17**:3636-3648

[45]Li L H, Dong W K, Zhang Y, et al. *Appl. Organomet. Chem.*, **2017**,**31**:e3818

[46]Ren Z L, Hao J, Hao P, et al. *Z. Naturforsch. B*, **2018**,**73**: 203-210

[47]Wang B J, Dong W K, Zhang Y, et al. *Sens. Actuators B*, **2017**,**247**:254-264

[48]Hao J, Li X Y, Zhang Y, et al. *Materials*, **2018**,**11**:523

[49]Wang F, Gao L, Zhao Q, et al. *Spectrochim. Acta Part A*, **2018**,**190**:111-115

[50]Dong W K, Li X L, Wang L, et al. *Sens. Actuators B*, **2016**, **229**:370-378

[51]Dong W K, Akogun S F, Zhang Y, et al. *Sens. Actuators B*, **2017**,**238**:723-734

[52]Zheng S S, Dong W K, Zhang Y, et al. *New J. Chem.*, **2017**, **41**:4966-4973

[53]Sun S S, Stern C L, Nguyen S T, et al. *J. Am. Chem. Soc.*, **2004**,**126**:6314-6326

[54]Sheldrick G M. *Acta Crystallogr. Sect. C*: *Cryst. Struct. Commun.*, **2015**,**C71**:3-8

[55]Yu B, Sun Y X, Yang C J, et al. *Z. Anorg. Allg. Chem.*, 2017,643:689-698

[56]GUO Jian-Qian(郭建强), SUN Yin-Xia(孙银霞), YU Bing(俞斌), et al. *Chinese J. Inorg. Chem.*(无机化学学报), **2017**, **33**:1481-1488

[57]Li J, Zhang H J, Chang J, et al. *Crystals*, **2018**,**8**:176

[58]ZHANG Hong-Jia(张宏佳), CHANG Jian(常健), JIA Hao-Ran(贾浩然), et al. *Chinese J. Inorg. Chem.*(无机化学学报), **2018**,**34**:2261-2270

[59]CHANG Jian(常健), ZHANG Hong-Jia(张宏佳), JIA Hao-Ran(贾浩然), et al. *Chinese J. Inorg. Chem.*(无机化学学报), **2018**,**34**:2097-2107

[60]Zhang L W, Liu L Z, Wang F, et al. *Molecules*, **2018**,**23**:1141

[61]Zhang H, Dong W K, Zhang Y, et al. *Polyhedron*, **2017**,**133**: 279-293

[62]Zhao Q, Wei Z L, Kang Q P, et al. *Spectrochim. Acta Part A*, **2018**,**203**:472-480

[63]Wang F, Liu L Z, Gao L, et al. *Spectrochim. Acta Part A*, **2018**,**203**:56-64

[64]Gao L, Liu C, Wang F, et al. *Crystals*, **2018**,**8**:77

[65]WANG Li(王莉), KANG Quan-Peng(康全鹏), HAO Jing(郝静), et al. *Chinese J. Inorg. Chem.*(无机化学学报), **2018**, **65**:893-899

[66]Dong X Y, Kang Q P, Li X Y, et al. *Crystals*, **2018**,**8**:139

[67]Kang Q P, Li X Y, Zhao Q, et al. *Appl. Organomet. Chem.*, **2018**,**32**:e4379

[68]McKinnon J J, Jayatilaka D, Spackman M A. *Chem. Commun.*, **2007**:3814-3816

[69]Martin A D, Hartlieb K J, Sobolev A N, et al. *Cryst. Growth Des.*, **2010**,**10**:5302-5306